Nanoscale Research Letters
a SpringerOpen Journal

NANO EXPRESS Open Access

Influences of graphene oxide support on the electrochemical performances of graphene oxide-MnO_2 nanocomposites

Huanping Yang[1], Jian Jiang[1], Weiwei Zhou[1], Linfei Lai[1], Lifei Xi[2], Yeng Ming Lam[2], Zexiang Shen[1], Bahareh Khezri[3] and Ting Yu[1,4*]

Abstract

MnO_2 supported on graphene oxide (GO) made from different graphite materials has been synthesized and further investigated as electrode materials for supercapacitors. The structure and morphology of MnO_2-GO nanocomposites are characterized by X-ray diffraction, X-ray photoemission spectroscopy, scanning electron microscopy, transmission electron microscopy, Raman spectroscopy, and Nitrogen adsorption-desorption. As demonstrated, the GO fabricated from commercial expanded graphite (denoted as GO(1)) possesses more functional groups and larger interplane gap compared to the GO from commercial graphite powder (denoted as GO(2)). The surface area and functionalities of GO have significant effects on the morphology and electrochemical activity of MnO_2, which lead to the fact that the loading amount of MnO_2 on GO(1) is much higher than that on GO(2). Elemental analysis performed via inductively coupled plasma optical emission spectroscopy confirmed higher amounts of MnO_2 loading on GO(1). As the electrode of supercapacitor, MnO_2-GO(1) nanocomposites show larger capacitance (307.7 F g^{-1}) and better electrochemical activity than MnO_2-GO(2) possibly due to the high loading, good uniformity, and homogeneous distribution of MnO_2 on GO(1) support.

Introduction

As one of the green supercapacitor electrode materials, MnO_2 shows potential to replace RuO_2 due to its high specific capacitance, environmental compatibility, low cost, and abundance in nature. In general, the fabrication of MnO_2 can be readily realized on large scale using traditional chemical co-precipitation methods [1,2]. However, MnO_2 powders produced by these methods suffer some disadvantages, like low specific surface area, and thus low specific capacitance in most cases. To improve the electrochemical performance, the strategy of direct deposition of MnO_2 on large-surface-area materials, such as carbon blacks, carbon nanotubes, activated or mesoporous carbons [3-9], is quite promising. Recently, graphene oxide (GO), a shining-star material, has been widely investigated as a suitable support for MnO_2 loading [10,11]. Thanks to the large accessible surface area provided by GO, more ions can transport onto the material surface, achieving high electric-double-layer capacitance in aqueous electrolytes. Furthermore, nanostructured MnO_2 modified on GO support can effectually prevent the aggregation of GO nanosheets caused by van der Waals interactions. As a result, the available electrochemical active surface area for energy storage can be greatly enhanced.

Structurally, a single-layer of graphite oxide, also called GO, consists of a honeycomb lattice of carbon atoms with oxygen-containing functional groups which are proposed to present in the form of carboxyl, hydroxyl, and epoxy groups [12,13]. These functional groups can enlarge the gap between adjacent GO sheets. For instance, the (002) diffraction peak of pristine graphite is located at approximately 26°, and the interplane distance is 0.34 nm. After oxidation of graphite, the diffraction peak shifts to a lower angle, indicative of a larger interplane gap. The functional groups and the larger interplane gap enable GO sheets to be easily decorated or intercalated by polymers, quantum dots, and metal/

* Correspondence: yuting@ntu.edu.sg
[1]Division of Physics and Applied Physics, School of Physical and Mathematical Sciences, Nanyang Technological University, 637371, Singapore, Singapore
Full list of author information is available at the end of the article

metal oxide nanoparticles (NPs), etc. [10,11,14-20], which are favorable and much desired for various applications. Nevertheless, until now, few reports have focused on the effects of functional groups and interplane gap of GO on the loading amount of quantum dots or metal/metal oxide nanoparticles, and so on.

In this work, we study the influences of GO supports on the electrochemical behavior of MnO_2-GO nanocomposites. Two types of GO nanosheets, denoted as GO(1) and GO(2), made from commercial expanded graphite (CEG) and commercial graphite powder (CGP), respectively, are employed as MnO_2 supports for comparative study. GO(1) nanosheets are proved to have more functional groups and larger interplane gap compared to GO(2) nanosheets, which might be capable of enhancing the loading amount of MnO_2. As a result, MnO_2-GO(1) nanocomposite exhibits higher energy and powder densities in neutral aqueous electrolytes.

Experimental

Materials

Commercial expanded graphite, commercial graphite powder, 98% H_2SO_4, 30% H_2O_2, potassium permanganate ($KMnO_4$) and $NaNO_3$ were used as received. Distilled water was used in all the processes of aqueous solution preparation and washing.

Material characterization

Scanning electron microscopy images were obtained on a field-emission scanning electron microscope (FE-SEM JEOL JSM-6700F; JEOL, Tokyo, Japan). Transmission electron microscopy (TEM) analyses were carried out using an electron microscope (JEM 2010F; JEOL, Tokyo, Japan) operating at 120 kV. The Raman spectra were recorded using a WITEC-CRM200 Raman system (WITEC, Germany). The excitation source is 532-nm laser (2.33 eV). X-ray photoelectron spectroscopy (XPS) measurement, was carried out on a thermo scientific ESCALAB 250 (Thermo Fisher Scientific, UK). The nanocomposites X-ray diffraction (XRD) studies were charactered by a Bruker D8 ADVANCE XRD (Bruker AXS, Germany). Nitrogen adsorption-desorption experiments were investigated at 77 K on an automatic volumetric sorption analyzer (Quantachrome, NOVA1200; Micromeritics, USA). The surface area was calculated using the Brunauer-Emmett-Teller equation. Pore size distributions were calculated by the Barrett-Joyner-Halenda (BJH) method using the adsorption branches. Quantitative elemental determinations were performed by firstly dissolving the solid samples with a CEM Mars microwave digester (Matthews, NC, USA), followed by analysis with a Thermo Scientific iCAP 6000 series inductively coupled plasma optical emission spectroscopy (ICP-OES, Thermo Scientific, England).

Synthesis of GO

Two kinds of graphite were used for synthesizing GO by a modified Hummers method [21-23]. In brief, 2 g of CEG (or CGP) and 1.5 g of $NaNO_3$ were added into 150 mL of 98% H_2SO_4 solution in a flask which was immersed in an ice bath. Afterwards, 9 g of $KMnO_4$ was slowly added in the solution. Meanwhile, the temperature of the mixed solution was maintained below 20°C for 2 h to avoid overheating and explosion. The mixture was stirred for 5 days. Then, 10 mL of 30% H_2O_2 was added into the solution in order to completely react with the remaining $KMnO_4$, leading to a bright yellow solution. Finally, the resulting mixture was washed by 3% H_2SO_4 and H_2O until the pH value of the solution was approximately 5-6. GO powder was obtained after freeze drying the suspension, labeled as GO(1)/GO(2).

Synthesis of MnO_2-GO nanocomposites

The MnO_2-GO nanocomposites were prepared by an *in situ* reduction method [24]. The detailed procedure was as follows: 200 mg of GO(1) (or GO(2)) was blended with 150 mL of 0.02 M $KMnO_4$ solution in a three-necked round-bottomed flask. The as-obtained mixture was refluxed at 120°C for 12 h with sustained magnetic stirring. The nanocomposites, labeled as MnO_2-GO(1) (or MnO_2-GO(2)), was then centrifuged, washed, and finally dried in air at 55°C overnight.

Electrochemical measurement

The working electrode of the electrochemical capacitors was fabricated by mixing the nanocomposites (15 mg) with 15 wt.% acetylene black and 5 wt.% polytetrafluoroene-ethylene binder of the total electrode mass. A small amount of ethanol was added to the mixture for more homogeneous paste. The mixture was then pressed onto nickel foam current collector (1.0 × 1.0 cm) (washed by acetone and 0.1 M HCl carefully before use) to make electrodes. Electrochemical characterizations were carried out in a conventional three-electrode cell with 1 M Na_2SO_4 as the electrolyte. A platinum foil and saturated Ag/AgCl electrode were used as the counter and reference electrode, respectively. All electrochemical measurements were conducted using CHI 660 electrochemical workstation.

Results and discussion

XRD patterns of CEG and CGP before and after oxidation are shown in Figure 1. As can be seen, the single peak at 2θ of 26.3° indicates the typical graphitic structure. Compared with CGP, the CEG shows a broad peak together with an upper shift of 0.4°, suggesting that CEG is amorphous and has a larger interlayer spacing. After chemical oxidation treatments, the GO(2) evolved from CGP still presents two XRD peaks corresponding

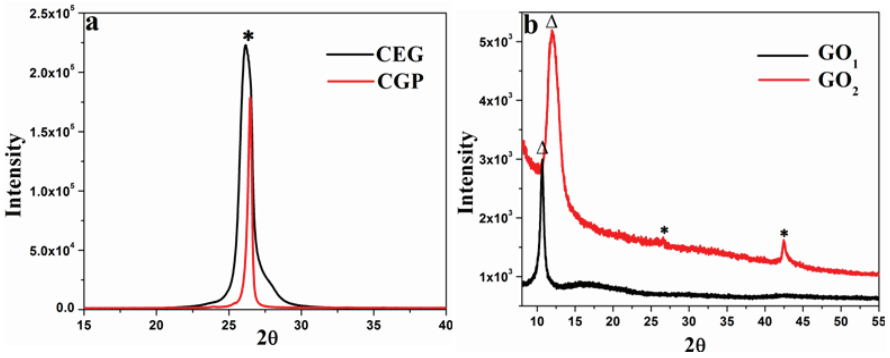

Figure 1 XRD of (a) CEG and CGP; (b) GO(1) and GO(2). Diffraction peaks of graphite* and GO $^{\Delta}$.

to the typical graphitic faces, whereas the pattern of GO (1) from CEG only shows one peak. Thus, the XRD results reveal that the CEG can be more easily exfoliated than CGP. Two diffraction peaks of GO(2) at approximately 26.3° and approximately 42.5° can be clearly seen from Figure 1b, corresponding to (002) and (101) planes of graphitic framework, respectively [25,26]. All peaks are weak and broad, which illustrate an amorphous carbon framework. This occurs because the interlayer spacing of the few-layered graphene sheet is similar to that of normal graphite, indicating that CGP has been partially converted into GO. In addition, there is a main peak at 2θ of 12.1° in GO(2) and 10.6° in GO(1), corresponding to d-spacing of 0.73 and 0.83 nm, respectively. This peak is similar to the typical diffraction peak of GO and is a possible indication of the presence of inter-few-layered graphene containing defects [27]. GO(1) has a larger interplane gap than GO(2), revealing its higher oxidation degree compared to GO(2).

Figure 2a and 2b reveal the morphology differences between CEG and CGP. CEG has bigger graphite piece than CGP, which leads to larger GO(1) sheets than GO (2) (Figure 2c and 2d). Figure 3a and 3b show that the MnO_2-GO(1) and MnO_2-GO(2) still maintain the skeleton structure of GO with diameters around 10 μm, even larger than pristine GO (Figure 2c and 2d). This means that after hydrothermal reaction, the nanocomposites became agglomerate. The TEM observations show the prepared nano-MnO_2 with morphology of nanorod and nanoflake uniformly decorated on the surface of the GO sheets. It is notable that both MnO_2 nanorods and nanoflakes can be found on GO(2). While for GO(1) support, there are only MnO_2 nanoflakes on its surface. Park and Keane have found that the strong epitaxial interaction between the catalytic species and the graphitic planes leads to a homogeneous distribution of the loaded Pd [28]. It is generally accepted that large interplanar spacing and high specific surface area of GO(1) would enhance the epitaxial interaction between nano-MnO_2 and the GO planes. As a result, MnO_2 nanoflakes can be distributed uniformly on GO(1) with smaller size than MnO_2 nanorods and nanoflakes on the GO(2) [29].

The inset HRTEM images in Figure 3 show the lattice fringes of the MnO_2-GO(1) and MnO_2-GO(2) nanocomposites. Three distinct sets of lattice spacing of ca. 0.237, 0.29, and 0.48 nm are shown, corresponding to the (211), (001), and (200) planes of α-MnO_2, respectively. The inset image in Figure 3a and 3 the upper inset image in Figure 3b present the orientation of the three epitaxial growths of MnO_2 nanoflakes on GO(1) and GO(2). Both epitaxial growths for the formation of the MnO_2 nanorods on GO(2) were revealed by the lower inset image in Figure 3b. The presence of clear lattice fringes in the HRTEM images confirms the crystalline nature of the α-MnO_2 nanorodes and nanoflakes. The following Raman and XPS characterization also prove the polymorph of the MnO_2 is α-MnO_2.

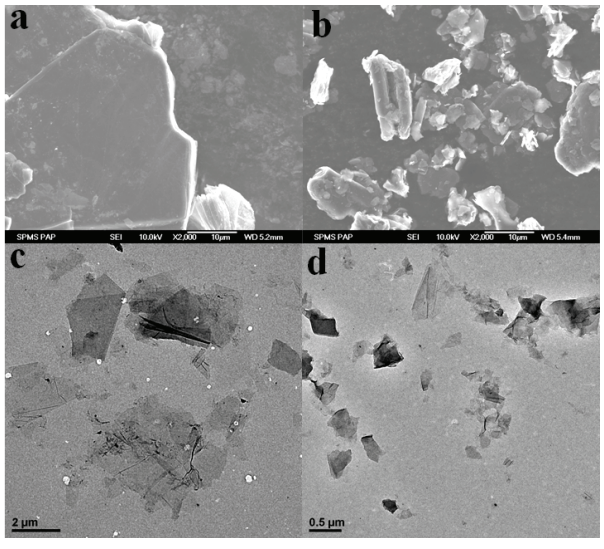

Figure 2 SEM (a b) and TEM (c d) images of: (a) CEG, (b) CGP, (c) GO(1) and (d) GO(2).

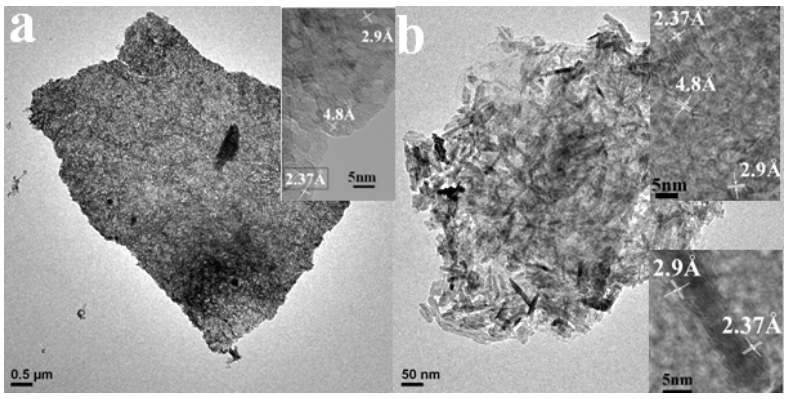

Figure 3 TEM and HRTEM images of (a) MnO_2-GO(1) and (b) MnO_2-GO(2).

The typical Raman spectra taken from different regions of the samples are shown in Figure 4. They present one diagnostic Raman scattering band of α-MnO_2, approximately 643 cm^{-1}, which belongs to A_g spectroscopic species originating from breathing vibrations of MnO_6 octahedra [30]. Two weak peaks recorded at approximately 305 and 360 cm^{-1} corresponding to the bending modes of O-Mn-O were observed in the spectra of the nanocomposites, stemming from the formation of Mn_2O_3 or Mn_3O_4 induced by the laser heating [31]. The appearance of a strong A_g-mode consists with our HRTEM result that the crystalline α-MnO_2 has been readily formed on the GO support. Another two prominent peaks, D band (1,345 cm^{-1}) and G band (1,597 cm^{-1}), belong to GO [32-35]. From Figure 4, we can also see that the ratio of α-MnO_2 to G is very different. MnO_2-GO(1) has a larger α-MnO_2 to G ratio than MnO_2-GO(2), which means that the content of MnO_2 in MnO_2-GO(1) is higher than that in MnO_2-GO (2). The Raman results are consistent with the inductively coupled plasma (ICP) and XPS results.

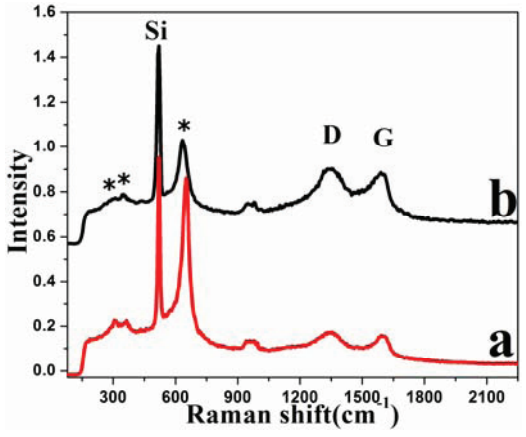

Figure 4 Raman Spectra of (a) MnO_2-GO(1) and (b) MnO_2-GO(2) sheets. (* α-MnO_2)

The element analysis was further studied by inductively coupled plasma (ICP) to prove the different amount of Mn in the nanocomposites. ICP-OES analysis of the concentrations of Mn in the nanocomposits confirmed that MnO_2-GO(1) (230.3 mg g^{-1}) has higher Mn content than MnO_2-GO(2) (153.6 mg g^{-1}), which will affect the morphology and electrochemical performances of the nanocomposites.

The nanocomposites obtained by using different GO sources have been further studied by the nitrogen adsorption-desorption measurements. As can be seen from Figure 5, all samples display a type-IV isotherm, indicating the mesoporous structure. Although MnO_2-GO(1) and MnO_2-GO(2) reveal the same type of the adsorption-desorption isotherm, their surface areas and pore size distributions are quite different. As for MnO_2-GO(1), the specific surface area and the total pore volume are measured to be approximately 238.1 m^2 g^{-1} and approximately 0.711 cm^3 g^{-1}, which are correspondingly larger than those for MnO_2-GO(2). Remarkably, these values are much higher than the data for MnO_2 produced by traditional co-precipitation of $KMnO_4$ and Mn^{2+}in previous report [36]. The pore size distribution plots of MnO_2-GO(1) and MnO_2-GO(2) are calculated by BJH method, using desorption branch of N_2 isotherms. MnO_2-GO(1) and MnO_2-GO(2) have comparable pore volumes. However, MnO_2-GO(2) shows narrower pore size distribution than MnO_2-GO(1), with a pore diameter range of 20-50 nm. The results clearly demonstrate that the graphite source has a significant effect on the microstructure of GO. The specific surface area and effective pores (8-50 Å) are reported to be effective to increase the double-layer capacitance of carbon and multiply the redox active sites for metal oxides loading. Therefore, the pseudo-capacitance will increase significantly. As a result, the unique structure could

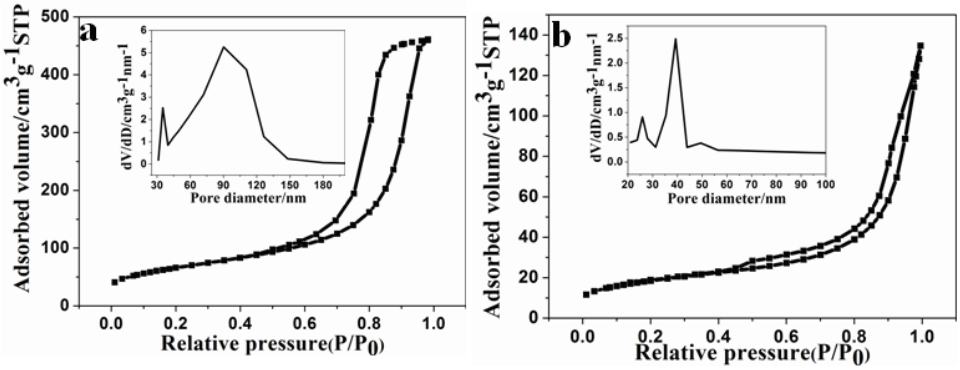

Figure 5 Nitrogen adsorption-desorption isotherms of (a) MnO_2-GO(1) and (b) MnO_2-GO(2). The inset shows BJH pore-size distributions.

be useful to enhance the capacity of MnO_2-GO(1) [24,37,38].

The high-resolution XPS spectra further confirm the different oxygen contents in GO(1) and GO(2), manganese contents and carbon contents in MnO_2-GO(1) and MnO_2-GO(2). As shown in Figure 6a and 6b, the curve fitting yields three components at sp^2-C (approximately 284.5 eV), C-O (hydroxyl and epoxy, approximately 286.5 eV), and C=O (carboxyl, approximately 288 eV), respectively [39-41]. The contribution of C=C band decreases from 50% for GO(2) to 40% for GO(1). An obvious broadening of C=C band is also observed, indicating a more disordered structure for GO(1), which agrees well with the XRD results.

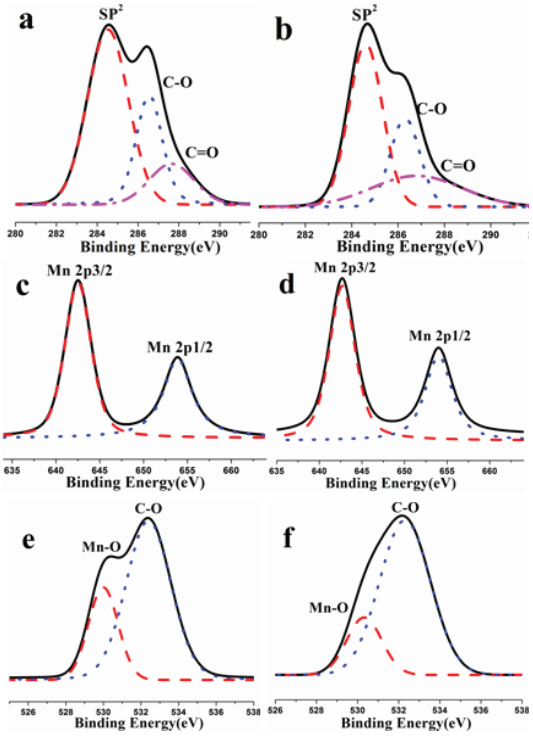

Figure 6 C1s spectra: (a) GO(1), (b) GO(2). (c-d) Mn2p, (e-f) O1s spectra of MnO2-GO(1) and MnO2-GO(2).

The spectra in Figure 6c and 6d illustrate the existence of MnO_2 by the peaks assigned to Mn 2p3/2 (642.7 eV) and Mn 2p1/2 (653.9 eV), respectively. They have a spin-energy separation of 11.2 eV, further confirming the presence of α-MnO_2 in the nanocomposite [42,43].

Besides the oxygen (O 1*s*, 532.4 eV) signals from graphene sheets in Figure 6e and 6f, the O 1*s* peak observed at 530.0 eV is assigned to the oxygen bonded with manganese [44]. On the basis of the quantitative analysis of XPS data, the corresponding atomic ratios of Mn to C for MnO_2-GO(1) and MnO_2-GO(2) in the nanocomposite are estimated to be 1:1.61 and 1:1.81 by integrating the area of each element peak areas, with their relative sensitive factor taken into account as well. It is worth noting that most carbon atoms in graphene sheets have not been substituted by Mn. However, MnO_2-GO(1) still has more replacement Mn position in the nanocomposite than MnO_2-GO(2). All of the data further confirm the existence of α-MnO_2 and the loading of MnO_2 is higher in MnO_2-GO(1) than that in MnO_2-GO(2).

The electrochemical performances of the GO obtained from different graphite sources before and after loading MnO_2 were investigated by cyclic voltammograms (CVs) and galvanostatic charge/discharge measurements in 1 M Na_2SO_4 solution between -0.3 and 0.8 V (Figure 7). From Figure 7a, it can be seen that the plots show an almost rectangular profile induced by an ideal capacitive behavior. GO shows lack of symmetry [43]. The poor electrochemical performance of GO is due to their poor electrical conductivity and low faradic reaction rate. However, the capacitance of GO(2) (21.39 F g^{-1}) is higher than that of GO(1) (0.64 F g^{-1}). Figure 7b shows the galvanostatic charge/discharge curves of the GO(1), GO(2), MnO_2-GO(1), and MnO_2-GO(2) at a current density of 100 mA g^{-1}. After MnO_2 loading, the capacity of MnO_2-GO(1) is twice that of MnO_2-GO(2) due to

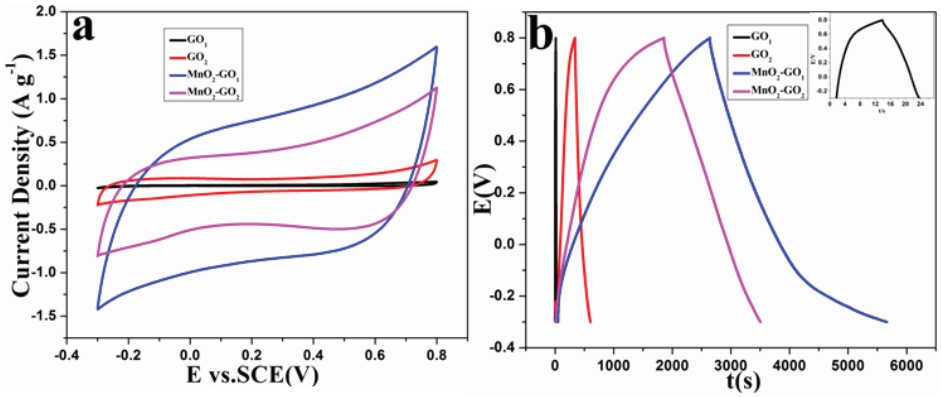

Figure 7 (a) CVs and (b) galvanostatic charge/discharge curves of GO(1), GO(2), MnO_2-GO(1), respectively.

the high loading amount of MnO_2 for GO(1) than that for GO(2).

Figure 8a and 8b show the CV curves of MnO_2-GO (1) and MnO_2-GO(2) nanocomposites. MnO_2-GO(1) shows the lack of symmetry at high scan rates (Figure 8b), which is probably due to pseudo-capacitance from MnO_2[10,43]. Specific capacitances of the nanocomposites calculated at current densities of 100, 250, 500 mA g^{-1} from the discharge curves are 176.0, 165.8, 140.3 F g^{-1} for MnO_2-GO(2) electrode, and 307.7, 297.3, 184.6 F g^{-1} for MnO_2-GO(1) electrode (Figure 8c and 8d). The MnO_2-GO(1) electrode has almost twice the specific capacitances of MnO_2-GO(2). The enhanced electrochemical performance of MnO_2-GO (1) electrode is due to the high MnO_2 loading by using the GO(1) with abundant surface functionalities. High loading and homogeneous distribution of MnO_2 on graphene oxide surface are advantageous for graphene oxide network to transport ions in the pore system and increasing the MnO_2-electrolyte interfacial area. Therefore, the excellent capability of GO(1) makes it attractive particularly for energy storage applications. Different GO precursors obviously have significant effect on the electrochemical capacitive performance before or after loading other nanomaterials. Thus, it is important to obtain highly porous and surface-functionalized graphene for supercapacitor applications.

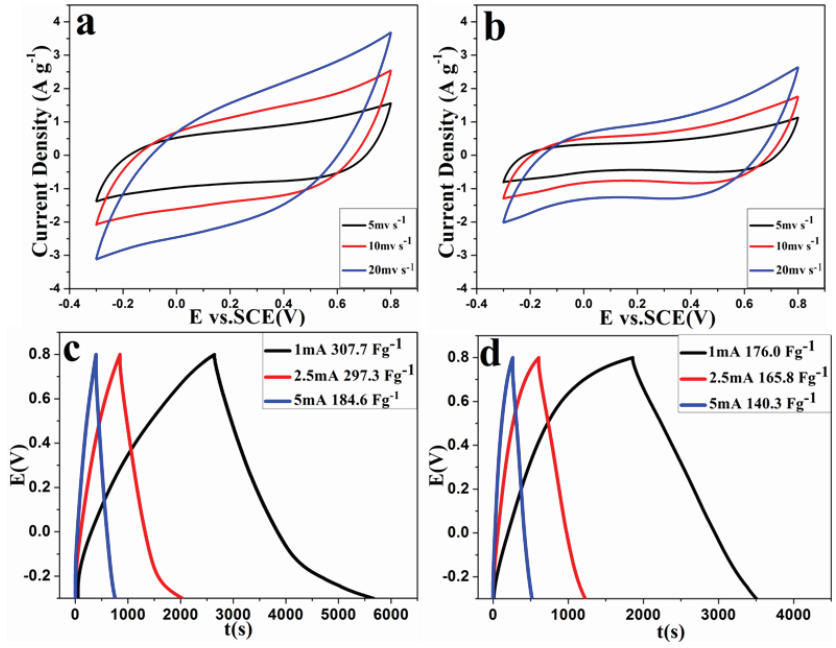

Figure 8 (a-b) CVs and (c-d) galvanostatic charge/discharge curves of MnO_2-GO(1) and (b) MnO_2-GO(2), respectively.

Conclusions

Based on the investigation of the chemical structure, morphology, and electrochemical behavior of MnO_2-GO (1) and MnO_2-GO(2), we conclude that the initial properties of GO have notable influences on the morphology and electrochemical activity of the GO-MnO_2 nanocomposites. The GO synthesized from the CEG has more functional groups and lager interplane distance. Therefore, MnO_2 nanoparticles can distribute homogeneously on GO(1) with high quantity. Because of the high surface area of MnO_2-GO(1) and high loading efficiency of MnO_2, the specific capacitance of MnO_2-GO(1) is almost twice of MnO_2-GO(2). The surface chemistry and structural properties of GO is of significant importance as nanoparticles carrier for various applications, such as catalyst, energy storage devices, etc.

Acknowledgements

This work is supported by the Singapore National Research Foundation under NRF RF Award no. NRF RF2010-07 and MOE Tier 2 MOE2009-T2-1-037. HPY gratefully thanks Professor Richard D. Webster for his fruitful discussions.

Author details

[1]Division of Physics and Applied Physics, School of Physical and Mathematical Sciences, Nanyang Technological University, 637371, Singapore, Singapore [2]School of Materials Science and Engineering, Nanyang Technological University, Nanyang Avenue, Singapore 639798, Singapore [3]Division of Chemistry and Biological Chemistry, School of Physical and Mathematical Sciences, Nanyang Technological University, 637371, Singapore, Singapore [4]Department of physics, Faculty of Science, National University of Singapore, 117542 Singapore, Singapore

Authors' contributions

HPY carried out the total experiment and write the manuscript. JJ participated in the detection of the supercapacitor. WZ participated in the detection of the SEM. LL participated in the detection of the BET and XPS. LX carried out the TEM detection. YML participated in the statistical analysis. ZS participated in the statistical analysis. BK carried out the detection of ICP. TY participated in the design of the study and performed the statistical analysis. All authors read and approved the final manuscript.

Competing interests

The authors declare that they have no competing interests.

Received: 14 June 2011 Accepted: 27 September 2011
Published: 27 September 2011

References

1. Toupin M, Brousse T, Belanger D: **Influence of microstucture on the charge storage properties of chemically synthesized manganese dioxide.** *Chem Mater* 2002, **14**:3946-3952.
2. Zhang ZA, Yang BC, Deng MG, Hu YD, Wang BH: **Synthesis and characterization of nanostructured MnO2 for supercapacitor.** *Acta Chimica Sinica* 2004, **62**:1617-1620.
3. Dong XP, Shen WH, Gu JL, Xiong LM, Zhu YF, Li Z, Shi JL: **MnO2-embedded-in-mesoporous-carbon-wall structure for use as electrochemical capacitors.** *J Phys Chem B* 2006, **110**:6015-6019.
4. Sharma RK, Oh HS, Shul YG, Kim H: **Carbon-supported, nano-structured, manganese oxide composite electrode for electrochemical supercapacitor.** *J Power Sourc* 2007, **173**:1024-1028.
5. Raymundo-Pinero E, Khomenko V, Frackowiak E, Beguin F: **Performance of manganese oxide/CNTs composites as electrode materials for electrochemical capacitors.** *J Electrochem Soc* 2005, **152**:A229-A235.
6. Prasad KR, Miura N: **Electrochemically synthesized MnO2-based mixed oxides for high performance redox supercapacitors.** *Electrochem Comm* 2004, **6**:1004-1008.
7. Fan Z, Chen JH, Wang MY, Cui KZ, Zhou HH, Kuang W: **Preparation and characterization of manganese oxide/CNT composites as supercapacitive materials.** *Diam Relat Mater* 2006, **15**:1478-1483.
8. Chen Y, Liu CG, Liu C, Lu GQ, Cheng HM: **Growth of single-crystal alpha-MnO2 nanorods on multi-walled carbon nanotubes.** *Mater Res Bull* 2007, **42**:1935-1941.
9. Malak-Polaczyk A, Matei-Ghimbeu C, Vix-Guterl C, Frackowiak E: **Carbon/lambda-MnO2 composites for supercapacitor electrodes.** *J Solid State Chem* 2010, **183**:969-974.
10. Liu FX, Cao ZS, Tang CJ, Chen L, Wang ZL: **Ultrathin diamond-like carbon film coated silver nanoparticles-based substrates for surface-enhanced raman spectroscopy.** *ACS Nano* 2010, **4**:2643-2648.
11. Wu ZS, Ren WC, Wang DW, Li F, Liu BL, Cheng HM: **High-energy MnO2 nanowire/graphene and graphene asymmetric electrochemical capacitors.** *ACS Nano* 2010, **4**:5835-5842.
12. Park S, Ruoff RS: **Chemical methods for the production of graphenes.** *Nature Nanotechnology* 2009, **4**:217-224.
13. Si Y, Samulski ET: **Synthesis of water soluble graphene.** *Nano Letters* 2008, **8**:1679-1682.
14. Li YG, Wu YY: **Coassembly of graphene oxide and nanowires for large-area nanowire alignment.** *J Am Chem Soc* 2009, **131**:5851-5857.
15. Kim H, Kim SW, Park YU, Gwon H, Seo DH, Kim Y, Kang K: **SnO2/graphene composite with high lithium storage capability for lithium rechargeable batteries.** *Nano Research* 2010, **3**:813-821.
16. Wang YY, Ni ZH, Hu HL, Hao YF, Wong CP, Yu T, Thong JTL, Shen ZX: **Gold on graphene as a substrate for surface enhanced Raman scattering study.** *Appl Phys Lett* 2010, **97.**
17. Fang M, Long LA, Zhao WF, Wang LW, Chen GH: **pH-responsive chitosan-mediated graphene dispersions.** *Langmuir* 2010, **26**:16771-16774.
18. Fu XQ, Bei FL, Wang X, O'Brien S, Lombardi JR: **Excitation profile of surface-enhanced Raman scattering in graphene-metal nanoparticle based derivatives.** *Nanoscale* 2010, **2**:1461-1466.
19. Liu JQ, Tao L, Yang WR, Li D, Boyer C, Wuhrer R, Braet F, Davis TP: **Synthesis, characterization, and multilayer assembly of pH sensitive graphene-polymer nanocomposites.** *Langmuir* 2010, **26**:10068-10075.
20. Zhou XZ, Huang X, Qi XY, Wu SX, Xue C, Boey FYC, Yan QY, Chen P, Zhang H: ***In situ* synthesis of metal nanoparticles on single-layer graphene oxide and reduced graphene oxide surfaces.** *J P Chem C* 2009, **113**:10842-10846.
21. Hernandez Y, Nicolosi V, Lotya M, Blighe FM, Sun ZY, De S, McGovern IT, Holland B, Byrne M, Gun'ko YK, Boland JJ, Niraj P, Duesberg G, Krishnamurthy S, Goodhue R, Hutchison J, Scardaci V, Ferrari AC, Coleman JN: **High-yield production of graphene by liquid-phase exfoliation of graphite.** *Nature Nanotechnology* 2008, **3**:563-568.
22. Hummers WS, Offeman RE: **Preparation of graphitic oxide.** *J Am Chem Soc* 1958, **80**:1339-1339.
23. Xu YX, Bai H, Lu GW, Li C, Shi GQ: **Flexible graphene films via the filtration of water-soluble noncovalent functionalized graphene sheets.** *J Am Chem Soc* 2008, **130**:5856-5857.
24. Xu MW, Jia W, Bao SJ, Su Z, Dong B: **Novel mesoporous MnO2 for high-rate electrochemical capacitive energy storage.** *Electrochimica Acta* 2010, **55**:5117-5122.
25. Fuertes AB, Alvarez S: **Graphitic mesoporous carbons synthesised through mesostructured silica templates.** *Carbon* 2004, **42**:3049-3055.
26. Kim TW, Park IS, Ryoo R: **A synthetic route to ordered mesoporous carbon materials with graphitic pore walls.** *Angew Chem Int Ed* 2003, **42**:4375-4379.
27. McAllister MJ, Li JL, Adamson DH, Schniepp HC, Abdala AA, Liu J, Herrera-Alonso M, Milius DL, Car R, Prud'homme RK, Aksay IA: **Single sheet functionalized graphene by oxidation and thermal expansion of graphite.** *Chem Mater* 2007, **19**:4396-4404.
28. Park C, Keane MA: **Catalyst support effects: gas-phase hydrogenation of phenol over palladium.** *J Colloid Interface Sci* 2003, **266**:183-194.
29. Qin HY, Liu ZX, Lao SJ, Zhu JK, Li ZP: **Influences of carbon support on the electrocatalysis of polypyrrole-modified cobalt hydroxide in the direct borohydride fuel cell.** *J Power Sourc* 2010, **195**:3124-3129.
30. Gao T, Fjellvag H, Norby P: **A comparison study on Raman scattering properties of alpha- and beta-MnO2.** *Anal Chim Acta* 2009, **648**:235-239.
31. Buciuman F, Patcas F, Craciun R, Zahn DRT: **Vibrational spectroscopy of bulk and supported manganese oxides.** *Phys Chem Chem Phys* 1999, **1**:185-190.

32. Su CY, Xu YP, Zhang WJ, Zhao JW, Liu AP, Tang XH, Tsai CH, Huang YZ, Li LJ: **Highly efficient restoration of graphitic structure in graphene oxide using alcohol vapors.** *ACS Nano* 2010, **4**:5285-5292.
33. Ni ZH, Wang YY, Yu T, Shen ZX: **Raman spectroscopy and imaging of graphene.** *Nano Research* 2008, **1**:273-291.
34. Su CY, Xu YP, Zhang WJ, Zhao JW, Tang XH, Tsai CH, Li LJ: **Electrical and spectroscopic characterizations of ultra-large reduced graphene oxide monolayers.** *Chem Mater* 2009, **21**:5674-5680.
35. Wu YH, Yu T, Shen ZX: **Two-dimensional carbon nanostructures: fundamental properties, synthesis, characterization, and potential applications.** *J Appl Phys* 2010, **108.**
36. Devaraj S, Munichandraiah N: **Effect of crystallographic structure of MnO2 on its electrochemical capacitance properties.** *J Phys Chem C* 2008, **112**:4406-4417.
37. Xu MW, Bao SJ, Li HL: **Synthesis and characterization of mesoporous nickel oxide for electrochemical capacitor.** *J Solid State Electrochem* 2007, **11**:372-377.
38. Xu MW, Zhao DD, Bao SJ, Li HL: **Mesoporous amorphous MnO2 as electrode material for supercapacitor.** *Journal of Solid State Electrochemistry* 2007, **11**:1101-1107.
39. Stankovich S, Dikin DA, Piner RD, Kohlhaas KA, Kleinhammes A, Jia Y, Wu Y, Nguyen ST, Ruoff RS: **Synthesis of graphene-based nanosheets via chemical reduction of exfoliated graphite oxide.** *Carbon* 2007, **45**:1558-1565.
40. Wang GX, Yang J, Park J, Gou XL, Wang B, Liu H, Yao J: **Facile synthesis and characterization of graphene nanosheets.** *J Phys Chem C* 2008, **112**:8192-8195.
41. Li Z, Zhang J, He HY, Bian JC, Zhang XW, Han GR: **Blue-green luminescence and SERS study of carbon-rich hydrogenated amorphous silicon carbide films with multiphase structure.** *Phys Status Solidi a-Applications and Materials Science* 2010, **207**:2543-2548.
42. Li QA, Liu JH, Zou JH, Chunder A, Chen YQ, Zhai L: **Synthesis and electrochemical performance of multi-walled carbon nanotube/polyaniline/MnO2 ternary coaxial nanostructures for supercapacitors.** *J Power Sourc* 2011, **196**:565-572.
43. Chen S, Zhu JW, Wang X: **From graphene to metal oxide nanolamellas: a phenomenon of morphology transmission.** *ACS Nano* 2010, **4**:6212-6218.
44. Sharma RK, Rastogi AC, Desu SB: **Manganese oxide embedded polypyrrole nanocomposites for electrochemical supercapacitor.** *Electrochimica Acta* 2008, **53**:7690-7695.

doi:10.1186/1556-276X-6-531
Cite this article as: Yang *et al.*: Influences of graphene oxide support on the electrochemical performances of graphene oxide-MnO_2 nanocomposites. *Nanoscale Research Letters* 2011 **6**:531.